



Article

Differential H₂O₂ Metabolism among Glioblastoma Subtypes Confers Variable Responses to Pharmacological Ascorbate Therapy Combined with Chemoradiation

Amira Zaher ¹, Kranti A. Mapuskar ¹, Jann N. Sarkaria ², Douglas R. Spitz ¹, Michael S. Petronek ^{1,*} and Bryan G. Allen ^{1,*}

¹ Department of Radiation Oncology, The University of Iowa, Iowa City, IA 52242, USA; amira-zaher@uiowa.edu (A.Z.); krantiashok-mapuskar@uiowa.edu (K.A.M.); douglas-spitz@uiowa.edu (D.R.S.)

² Department of Radiation Oncology, Mayo Clinic, Rochester, MN 55905, USA; sarkaria.jann@mayo.edu

* Correspondence: michael-petronek@uiowa.edu (M.S.P.); bryan-allen@uiowa.edu (B.G.A.)

Abstract: Glioblastoma (GBM), a highly lethal and aggressive central nervous system malignancy, presents a critical need for targeted therapeutic approaches to improve patient outcomes in conjunction with standard-of-care (SOC) treatment. Molecular subtyping based on genetic profiles and metabolic characteristics has advanced our understanding of GBM to better predict its evolution, mechanisms, and treatment regimens. Pharmacological ascorbate (P-AscH⁻) has emerged as a promising supplementary cancer therapy, leveraging its pro-oxidant properties to selectively kill malignant cells when combined with SOC. Given the clinical challenges posed by the heterogeneity and resistance of various GBM subtypes to conventional SOC, our study assessed the response of classical, mesenchymal, and proneural GBM to P-AscH⁻. P-AscH⁻ (20 pmol/cell) combined with SOC (5 μM temozolomide and 4 Gy of radiation) enhanced clonogenic cell killing in classical and mesenchymal GBM subtypes, with limited effects in the proneural subtype. Similarly, following exposure to P-AscH⁻ (20 pmol/cell), single-strand DNA damage significantly increased in classical and mesenchymal but not proneural GBM. Moreover, proneural GBM exhibited increased hydrogen peroxide removal rates, along with increased catalase and glutathione peroxidase activities compared to mesenchymal and classical GBM, demonstrating an altered H₂O₂ metabolism that potentially drives differential P-AscH⁻ toxicity. Taken together, these data suggest that P-AscH⁻ may hold promise as an approach to improve SOC responsiveness in mesenchymal GBMs that are known for their resistance to SOC.

Keywords: glioblastoma; chemoradiation; glioblastoma subtypes; pharmacological ascorbate; antioxidant therapy; prooxidant; hydrogen peroxide; DNA damage



Citation: Zaher, A.; Mapuskar, K.A.; Sarkaria, J.N.; Spitz, D.R.; Petronek, M.S.; Allen, B.G. Differential H₂O₂ Metabolism among Glioblastoma Subtypes Confers Variable Responses to Pharmacological Ascorbate Therapy Combined with Chemoradiation. *Int. J. Mol. Sci.* **2023**, *24*, 17158. <https://doi.org/10.3390/ijms242417158>

Academic Editor: José Ángel Campos Sandoval

Received: 2 November 2023

Revised: 29 November 2023

Accepted: 4 December 2023

Published: 5 December 2023



Copyright: © 2023 by the authors. Licensee MDPI, Basel, Switzerland. This article is an open access article distributed under the terms and conditions of the Creative Commons Attribution (CC BY) license (<https://creativecommons.org/licenses/by/4.0/>).

1. Introduction

Glioblastoma (GBM) is the most common and aggressive adult primary brain malignancy, with approximately 14,000 cases diagnosed annually [1–4]. GBM has poor clinical outcomes, with a 5-year overall survival rate of less than 10% [1–3]. The current standard of care (SOC) for GBM consists of maximum safe surgical resection followed by radiation therapy and temozolomide (TMZ) [3]. Unfortunately, effective treatment options for GBM are faced with multiple challenges, including radiation resistance and radiation-induced brain injury, the blood–brain barrier, and tumor heterogeneity. GBM tumors are often resistant to radiation due to altered metabolism, hypoxia, and increased DNA repair capacity [5,6]. Moreover, radiation therapy is known to induce a variety of injuries to the brain, ranging from neuroinflammation and cognitive dysfunction to dementia [7,8]. The blood–brain barrier is altered in GBM due to the interference of tumor vasculature; this alteration contributes to hypoxia and confers resistance to chemotherapeutic agents such

as TMZ [9–11]. These challenges underscore the urgent need for innovative approaches to sensitize GBM to SOC therapy.

Recently, pharmacological ascorbate (high-dose intravenous infusions of vitamin C resulting in plasma concentrations of ≈ 20 mM, P-AscH⁻) has garnered attention as a potential anticancer agent to enhance the response to SOC therapy across various malignancies, including GBM [12–16]. When ascorbate is oxidized, it generates high levels of hydrogen peroxide (H₂O₂), which can react with redox-active iron, primarily Fe²⁺, through Fenton chemistry, resulting in an excess of damaging hydroxyl radicals capable of disrupting biological macromolecules [12,13,16,17]. Since malignant cells are believed to exhibit altered mitochondrial function, leading to increased steady-state levels of reactive oxygen species, increased iron concentrations, and reduced levels of antioxidant enzymes (e.g., catalase), P-AscH⁻ is hypothesized to be a selective pro-oxidant in cancer cells relative to their non-malignant counterparts [16–18]. Recently, a phase 2 clinical trial demonstrated that P-AscH⁻ enhanced SOC clinical outcomes in GBM patients increasing overall survival to 19.6 months [16,19]. However, a subset of subjects receiving P-AscH⁻ was unresponsive, prompting the need to identify biologically relevant factors driving P-AscH⁻ response.

GBM subtypes, classified based on their transcriptional profiles into mesenchymal, classical, and proneural subtypes, offer a potential avenue for refining GBM therapy. While IDH mutational status and O⁶-methylguanine-DNA methyltransferase (MGMT) methylation are primary considerations in GBM treatment, GBM molecular subtypes are currently underemphasized in patient evaluation. Nonetheless, earlier studies revealed that GBM subtypes exhibit distinct clinical outcomes, metabolic characteristics, and immune signatures [20,21]. Additionally, it has been observed that patient prognosis varies among subtypes, with proneural and classical GBMs demonstrating a more favorable outlook compared to mesenchymal tumors [20–22]. Consequently, these subtype-related distinctions present an opportunity to guide the utilization of P-AscH⁻ therapy in GBM. This study aimed to conduct the first preclinical assessments of the response of mesenchymal, classical, and proneural GBM subtypes to P-AscH⁻ therapy, while also investigating potential disparities in H₂O₂ metabolism contributing to their varying responses, thus providing a novel insight into GBM H₂O₂ metabolism in the context of P-AscH⁻ therapy.

2. Results

2.1. Glioblastoma Subtypes Exhibit a Differential Response to P-AscH⁻ with SOC

The cytotoxic effect of combining P-AscH⁻ with SOC (5 μ M TMZ and 4 Gy IR) in the three GBM subtypes was initially assessed using a colony formation assay (Figure 1D). The addition of P-AscH⁻ significantly augmented the cytotoxicity of SOC in classical GBM cells compared to SOC treatment alone (mean = 0.25, 0.41, respectively, $p = 0.001$; see Figures 1A and S1A,B). Interestingly, mesenchymal GBMs, often associated with treatment resistance, displayed a substantial enhancement in cell killing when treated with SOC + P-AscH⁻ compared to SOC alone (means = 0.25, 0.51, respectively, $p = 0.0009$, Figures 1B and S1C–E). The change in cell survival between SOC and SOC + P-AscH⁻ was more pronounced in mesenchymal GBM cells than in classical GBM cells (Δ NSF = 0.26, 0.16, respectively). These findings suggest that mesenchymal GBMs are more sensitive to P-AscH⁻ therapy compared to classical GBMs. P-AscH⁻ did not enhance the cytotoxic effects of SOC in proneural GBMs (Figures 1C,D and S1F,G). These data underscore the distinct responses to P-AscH⁻ observed within different GBM subtypes.

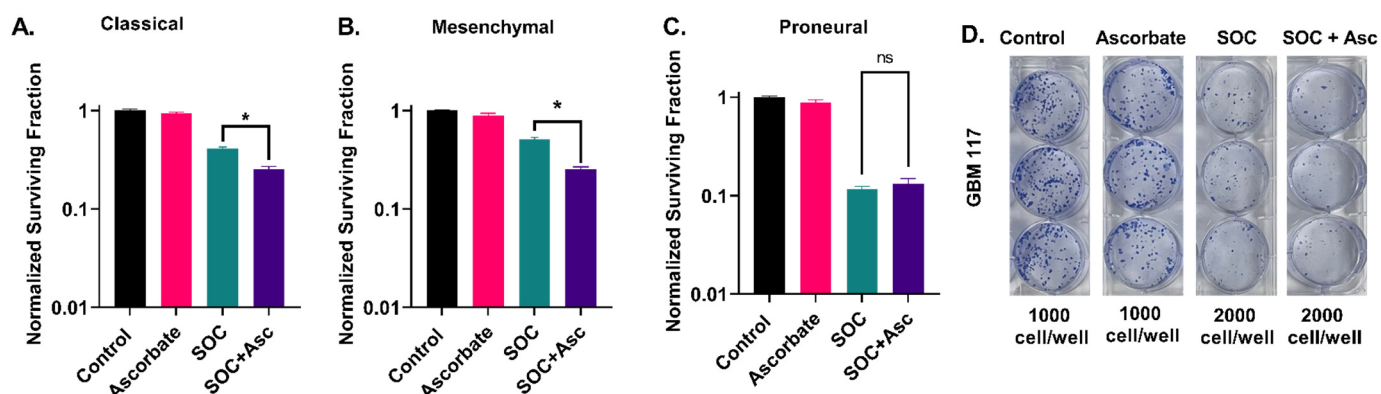


Figure 1. The effect of P-AscH⁻ on colony formation in different GBM subtypes treated with SOC. (A). P-AscH⁻ significantly enhanced SOC in classical GBM. Data are shown from GBM06 and GBM76. (B). SOC in mesenchymal GBM was significantly enhanced by the addition of P-AscH⁻. Data presenting U87, U251, and GBM39. (C). P-AscH⁻ did not show differences in response to SOC in proneural GBM. Data are shown from GBM117 and GBM85. (D). Representative images showing GBM117 colonies treated with SOC and SOC + P-AscH⁻. * is statistically significant, $p < 0.05$. ns, not significant. Data show normalized survival fractions from 3 replicates in each cell line. Error bars represent the standard error of the mean (SEM).

2.2. DNA Damage Responses following P-AscH⁻ Treatments Are Subtype-Dependent

DNA damage is a recognized primary mechanism for cell destruction induced by both radiation and temozolomide. Therefore, the impact of P-AscH⁻ on the induction of DNA damage was evaluated within this model system. Previous research showed that P-AscH⁻ induces single-strand DNA breaks through site-specific oxidations via hydroxyl radicals [23–25]. Thus, it was hypothesized that the induction of single-stranded DNA damage by P-AscH⁻ might occur in a subtype-specific pattern, similar to the in vitro enhancement of SOC.

Consistent with the observed cell-killing effects (Figure 1), P-AscH⁻ significantly increased single-stranded DNA damage in both classical and mesenchymal GBM cells. This effect was not observed in proneural GBMs ($p = 0.006$, 0.017 , and 0.24 , respectively; Figures 2A and S2A–E). Notably, P-AscH⁻ induced the highest level of single-strand DNA breaks in classical GBM when compared to mesenchymal and proneural GBMs (37.5%, 18.9%, and 14.4%, respectively; Figures 2A and S2A–F). These results align with the subtype-specific enhanced cell-killing effects of P-AscH⁻ and emphasize the diverse responses within different GBM subtypes. We also assessed the induction of double-stranded DNA breaks. Classical GBMs showed a significant increase in double-stranded DNA breaks ($p = 0.018$) with P-AscH⁻ (Figures 2B and S3C). In contrast, this effect was not observed in mesenchymal or proneural GBMs ($p = 0.78$, and 0.97 , respectively; Figures 2B and S3A,B,D,F). These results align with the subtype-specific enhanced cell-killing effects of P-AscH⁻ and underscore the potential significance of DNA damage as a central mechanism of action.

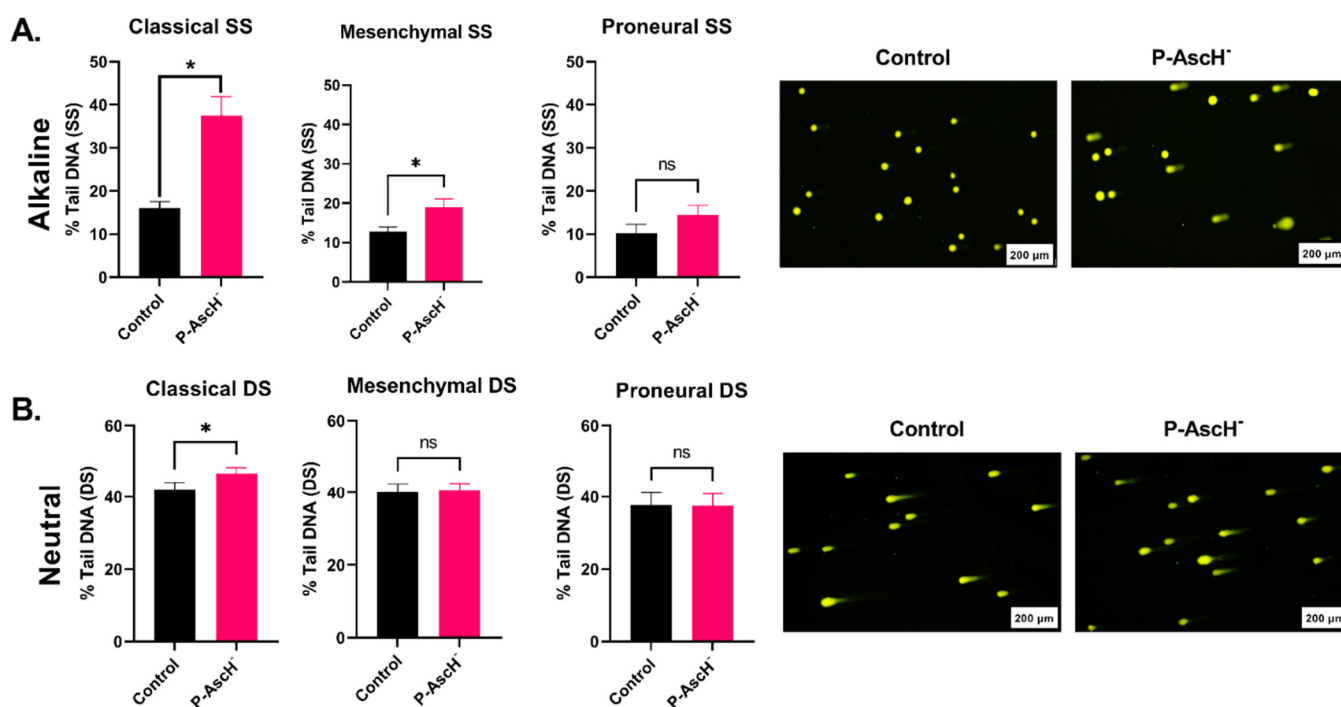


Figure 2. DNA damage following 1 h treatment with 20 pmol/cell P-AscH⁻. Classical (GBM06 and GBM76), mesenchymal (U87, U251, GBM39), and proneural (GBM117) data are shown. (A). Single-strand DNA breaks as % tail DNA in GBM subtypes following P-AscH⁻ treatment using the alkaline comet assay. Representative images (right) showing alkaline comets in GBM06 cells. (B). Double-strand breaks as % tail DNA in GBM subtypes following P-AscH⁻ treatment using the neutral comet assay. Representative images (right) showing neutral comets in GBM117 cells. The scale on all representative images is 200 μm . * is statistically significant, $p < 0.05$. ns, not significant. Data are shown from 3 replicates in each cell line. Error bars represent the standard error of the mean (SEM).

2.3. GBM Subtypes Exhibit Subtype-Dependent Differences in Hydrogen Peroxide Metabolism

H₂O₂ is considered the primary mediator of P-AscH⁻ cancer cell toxicity due to its ability to react with redox-active iron, leading to DNA oxidative damage [16,17,26–29]. Since P-AscH⁻ has been demonstrated to enhance the cell-killing effects of SOC and induce DNA damage in a subtype-dependent manner (Figures 1 and 2), we hypothesized that H₂O₂ metabolism varied amongst the three GBM subtypes.

The classical subtype had the lowest rate of H₂O₂ removal ($5.2 \times 10^{-12} \text{ s}^{-1} \text{ cell}^{-1} \text{ L}$) in comparison to both mesenchymal ($8.5 \times 10^{-12} \text{ s}^{-1} \text{ cell}^{-1} \text{ L}$, $p = 0.476$), and proneural cells ($21.2 \times 10^{-12} \text{ s}^{-1} \text{ cell}^{-1} \text{ L}$, $p = 0.0001$; Figure 3A and Table S1). Given the observed differences in the rate of H₂O₂ removal amongst the subtypes, we examined the enzymatic activity of both catalase (Cat) and glutathione peroxidase (GPx). Cat and GPx both play central roles in H₂O₂ metabolism. No significant differences were observed in the mesenchymal and proneural cells in either Cat ($p = 0.52$) or GPx ($p = 0.99$) activity (Figure 3B,C). However, classical GBMs showed significantly lower CAT activity in comparison to both mesenchymal and proneural GBM cells ($p = 0.0003$, and 0.0124 , respectively; Figures 3B,C and S4A,B). Significantly lower GPx activity was also observed in classical GBM cells compared to both mesenchymal and proneural cells ($p = 0.01$ and 0.03 , respectively; Figures 3B,C and S4A,B). Following the assessment of H₂O₂ metabolism in GBM subtypes, it appears that they have different capacities to remove H₂O₂ which can be attributed to the differential activities of Cat and GPx among the different subtypes. However, it is noteworthy that the differences in H₂O₂ metabolism between mesenchymal and proneural GBM may not be the sole factor responsible for mediating P-AscH⁻ toxicity and inducing DNA damage.

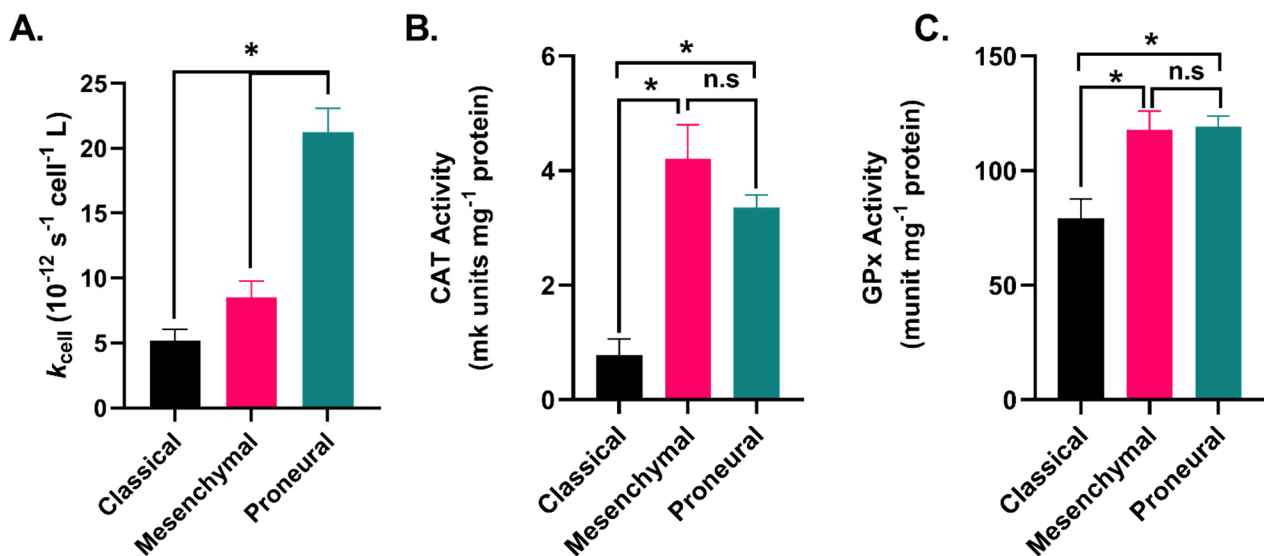


Figure 3. Differential H_2O_2 metabolism in GBM subtypes. (A). Hydrogen peroxide removal rates ($10^{-12} \text{ s}^{-1} \text{ cell}^{-1} \text{ L}$) in GBM subtypes). Classical (GBM06 and GBM76), mesenchymal (U87, U251, GBM39), and proneural (GBM117 and GBM117) data are shown (B). Catalase activity (mk units per mg protein) in GBM subtypes. Classical (GBM06 and GBM76), mesenchymal (U251 and GBM39), and proneural (GBM117) data are shown. (C). GPx1 activity (munit per mg protein) in GBM subtypes. Classical (GBM06 and GBM76), mesenchymal (U251 and GBM39), and proneural (GBM117) data are shown. Data are shown from 3 replicates per cell line. * is statistically significant, $p < 0.05$. ns, not significant. Data are shown from 3 replicates in each cell line. Error bars represent the standard error of the mean (SEM).

2.4. Increased P-AscH⁻ Dosing Further Improves Overall Survival in a Murine Xenograft Model of Mesenchymal GBM

Mesenchymal GBMs are well known for their aggressive nature and resistance to SOC treatment [30,31]. Since P-AscH⁻ significantly improves the response to SOC and induced DNA damage in mesenchymal GBM cells in vitro, we postulated that P-AscH⁻ could enhance SOC therapy in vivo and that the frequency of P-AscH⁻ dosing played a crucial role in response. We conducted a study comparing the overall survival of mice bearing mesenchymal U87 xenografts treated with SOC \pm P-AscH⁻ using two separate P-AscH⁻ dosing schedules as outlined in Table 1. Sequence 1 dosed P-AscH⁻ three days per week, while Sequence 2 dosed ascorbate five days per week.

Table 1. Treatment groups, doses, and frequency of treatment.

Phase	Active Treatment (2 Weeks)			Adjuvant Phase (2 Weeks)			
	Treatment	IR	TMZ	P-AscH ⁻	IR	TMZ	P-AscH ⁻
Control	-	-	-	-	-	-	-
SOC	2 Gy \times 3 weekly.	2.5 mg kg^{-1} weekly	-	-	2.5 mg kg^{-1} weekly	-	-
Sequence 1	2 Gy \times 3 weekly.	2.5 mg kg^{-1} weekly	4 g kg^{-1} \times 3 weekly	-	2.5 mg kg^{-1} weekly	4 g kg^{-1} weekly	-
Sequence 2	2 Gy \times 3 weekly.	2.5 mg kg^{-1} weekly	4 g kg^{-1} \times 5 weekly	-	2.5 mg kg^{-1} weekly	4 g kg^{-1} weekly	-

Both Sequence 1 and Sequence 2 resulted in a significant reduction in tumor growth rates compared to SOC treatment alone ($p = 0.005$ and 0.0009 , respectively). However, there were no significant differences in tumor growth between Sequence 1 and Sequence 2 ($p > 0.9999$; Figure 4A). Animals were observed for up to 66 days post treatment to assess overall survival. While there were no discernible differences in tumor growth

between Sequence 1 and 2 (Figure 4A), Sequence 2 significantly improved overall survival when compared to both SOC alone and Sequence 1 ($p = 0.0002$ and 0.027 , respectively; Figure 4B). Body weight changes across all groups followed a similar pattern (Figure 4C), with no notable body weight changes observed with additional P-AscH⁻ doses. These findings are in line with our previously reported data in an orthotopic U87 model, thus demonstrating the capacity of P-AscH⁻ to enhance SOC in both a flank and an orthotopic model [19]. Collectively, these data support the notion that P-AscH⁻ represents a promising strategy for enhancing SOC therapy and that increased dosing of P-AscH⁻ enhances GBM tumor control.

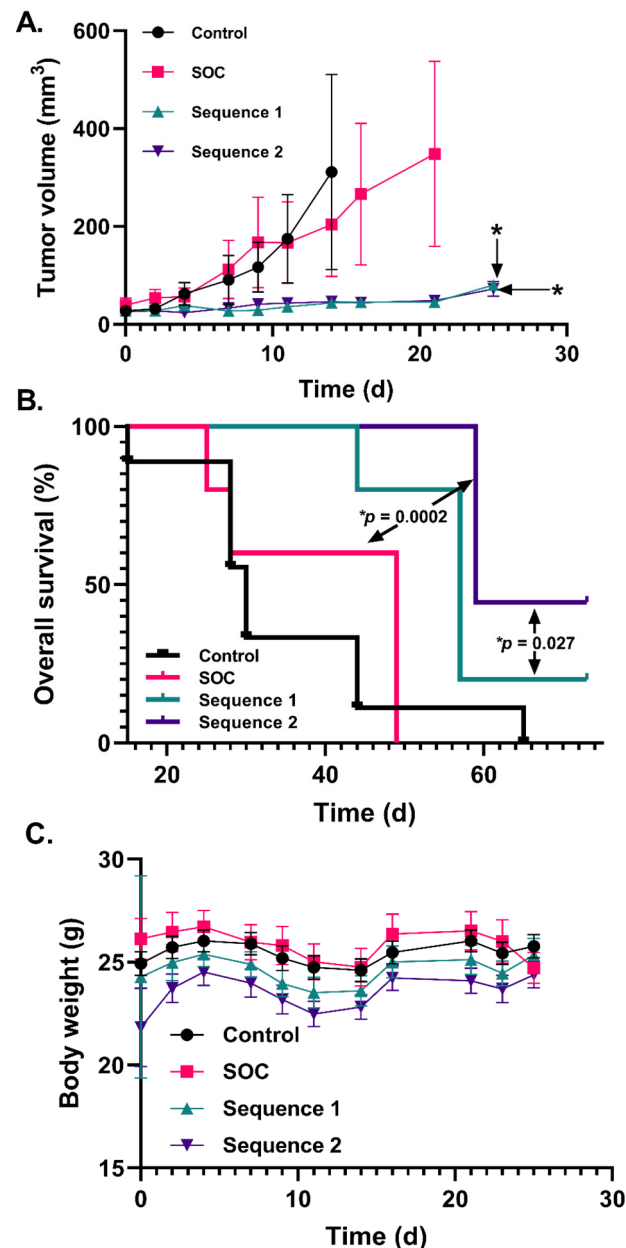


Figure 4. Increasing P-AscH⁻ doses in mesenchymal GBM further enhances overall survival in a xenograft mouse model. Control (n = 10), SOC (n = 6), Sequence 1 (n = 5), Sequence 2 (n = 9). (A). Tumor growth rate of U87 xenografts with SOC compared to P-AscH⁻ 3 times/week and 5 times/week. (B). Percent overall survival in mice with U87 tumors following treatment with the addition of P-AscH⁻ 3 days per week or 5 days per week. (C). Body weights in grams (g) of mice in the control group and the 3 treatment groups showed no significant changes in body weight. * is statistically significant, $p < 0.05$. Error bars represent the standard error of the mean (SEM).

3. Discussion

P-AscH⁻ is hypothesized to exhibit antioxidant properties in non-malignant tissue while acting as a cytotoxic pro-oxidant agent in cancerous tissue [12,16,17,29]. Recent clinical data have shown promising outcomes for GBM patients treated with P-AscH⁻ [16,19]. Given the significance of these findings, this study aimed to gain insights into how different GBM subtypes respond to P-AscH⁻ therapy, potentially guiding future clinical applications of P-AscH⁻ in conjunction with SOC. We present evidence that P-AscH⁻ significantly enhances the response to SOC in classical and mesenchymal GBM, whereas this effect is not observed in proneural GBM. Our clonogenic survival data demonstrated that P-AscH⁻ enhances the response to SOC exclusively in classical and mesenchymal GBM cells, with both subtypes exhibiting significant increases in single-stranded DNA breaks. Only classical GBMs had a significant increase in double-stranded DNA breaks. Thus, classical GBM cells were the most sensitive to DNA damage induced by P-AscH⁻. Although P-AscH⁻ is primarily believed to affect DNA through the induction of single-strand breaks [23–25], it is conceivable that double-strand breaks are also created due to spontaneous generation or impaired DNA repair processes or close proximity of single-strand breaks, suggesting that classical GBMs may possess defective DNA repair machinery that promotes the persistence of single-strand breaks into double-strand breaks [32,33]. Interestingly, these findings reveal that P-AscH⁻ responses do not consistently align with the known prognostic outcomes of these subtypes, as proneural tumor cells often exhibit increased therapeutic sensitivity to SOC [21,22]. In summary, our study highlights the GBM subtype-specific effectiveness of P-AscH⁻ in vitro which is strongly associated with the induction of DNA damage.

To elucidate the differential responses to P-AscH⁻, we evaluated H₂O₂ metabolism in the three GBM subtypes. Proneural GBM cells had a high H₂O₂ removal rate along with elevated Cat and GPx activities. These results are consistent with proneural cell resistance to P-AscH⁻ therapy which can be attributed to their proficient H₂O₂ removal capacity. In contrast, classical GBM cells demonstrated decreased H₂O₂ removal rates and Cat and GPx activities compared to mesenchymal and proneural GBM cells, indicating an enhanced sensitivity to P-AscH⁻-induced DNA damage. This suggests that in classical GBM cells, Cat and GPx enzymes may play a more significant role in modulating responses to H₂O₂. Although mesenchymal GBM cells exhibited significantly lower H₂O₂ removal rates compared to proneural GBM, no differences were observed in their CAT and GPx activities. The distinct response patterns of these two subtypes may be attributed to other components of the antioxidant enzyme machinery, such as peroxiredoxins or superoxide dismutases [16,34]. Another contributing factor to the differential responses to P-AscH⁻ is the intracellular availability of Fe²⁺, which we have observed to be a major driver of P-AscH⁻ toxicity in GBM [16,35]. In aggregate, the differences in H₂O₂ metabolism between mesenchymal and proneural GBMs appear to be multifaceted, warranting further investigation to address other antioxidant enzymes and iron metabolic alterations. Mesenchymal GBMs are known for their poor prognosis due to their enhanced resistance to chemotherapy and radiotherapy as prior studies indicated that the transition from a proneural to a mesenchymal subtype promotes a therapy-resistant phenotype [30,31]. Our study demonstrated encouraging responses to P-AscH⁻ in mesenchymal GBM cells, which, when combined with SOC, increased susceptibility to P-AscH⁻-induced DNA damage.

Previously, GBM patients were administered 82.6 g ascorbate infusions three times a week, resulting in plasma ascorbate concentrations of ≈20 mM [16,19]. In this study, we utilized a previously established P-AscH⁻ dosing model (4 g kg⁻¹) that was shown to enhance GBM response to standard of care therapy in flank and orthotopic GBM xenografts [16,19]. This study aimed to evaluate if P-AscH⁻ dosing frequency had an impact on tumor control. The concentrations of AscH⁻ achieved in the central nervous system through pharmacological dosing remain unclear; however, concentrations in the cerebrospinal fluid are known to be approximately 3.5–4.5 times greater than those observed in plasma [36–38]. Thus, it can be speculated that AscH⁻ concentrations in the cerebrospinal fluid following P-AscH⁻ administration may reach ≥20 mM, which may be a key contributing factor to the

successful application of P-AscH⁻ in the context of GBM. In U87 tumors, we observed that increasing the frequency of P-AscH⁻ administration with SOC from three days per week to five days per week during the active treatment phase significantly improved overall survival without inducing significant toxicities. These preclinical findings suggest that GBM patients with mesenchymal tumors may benefit from increased P-AscH⁻ dosing regimens, thus potentially guiding the design of future P-AscH⁻ clinical trials. Additionally, mesenchymal GBMs exhibit a unique and robust tumor microenvironment, enriched with tumor-associated macrophages [31,39], presenting another potential mechanism of P-AscH⁻ that has yet to be comprehensively explored in GBM [15]. In conclusion, this study highlights the potential role of the GBM subtype as a biomarker for P-AscH⁻ therapy. The observed variability in H₂O₂ metabolism across these subtypes necessitates further investigation, given the clinical demand for effective GBM treatment strategies.

4. Materials and Methods

4.1. Cell Lines

All GBM cells (Table 2) were cultured in DMEM-F12 media with the following additives: 15% FBS, 1% penicillin-strep, 1% Na-pyruvate, 1.5% HEPES, 0.1% insulin, and 0.02% fibroblast growth factor. Cells were maintained at 37 °C with 5% CO₂. All experiments were performed at 4% O₂ and 70–80% cell confluency.

Table 2. Characteristics of cell lines used in this study.

Cell Line	Source	Subtype	Sex	IDH Status	MGMT Methylation
U251	Millipore Sigma	Mesenchymal	M	Wild-type	Unmethylated
U87	ATCC	Mesenchymal	M	Wild-type	Unmethylated
* GBM06	Primary tumor	Classical	M	Wild-type	Unmethylated
* GBM76	Recurrent tumor	Classical	M	Wild-type	Methylated
* GBM39	Primary tumor	Mesenchymal	M	Wild-type	Methylated
* GBM117	Primary tumor	Proneural	M	Wild-type	Methylated
* GBM85	Primary tumor	Proneural	M	Wild-type	Methylated

* Cells obtained from the Mayo Clinic GBM patient-derived xenograft repository.

4.2. Colony Formation Assay

To determine the effect of P-AscH⁻ in conjunction with SOC on reproductive integrity in the different GBM subtypes, classical, mesenchymal, and proneural cells were plated at $1\text{--}2 \times 10^5$ cells per 60 mm dish. Within 24 h of plating, cells were serially treated with 5 μM temozolomide for 1 h and 20 pmol/cell P-AscH⁻ for 1 h and were irradiated with 4 Gy. Subsequently, cells from control or treated dishes were collected by treatment with trypsin (0.25%). Trypsin was inactivated with BR15 media containing 15% FBS and additives. Cell counts were made with a Coulter Counter and the cells were plated at various densities and allowed to grow for 1–4 weeks in complete media at 4% O₂. Subsequently, the cells were stained with Coomassie Blue dye, colonies greater than 50 cells per plate were counted and recorded, and clonogenic cell survival was determined as described previously [40]. The surviving fraction was determined using the following equation:

$$\text{Surviving Fraction} = \frac{\text{number of colonies counted}}{\text{number of cells plated}}$$

Treatment groups were normalized to an untreated control to determine the normalized surviving fraction (NSF).

4.3. P-AscH⁻ Treatments

A 1M stock solution of ascorbic acid was used in all experiments. For in vitro studies, cells on a dedicated “count” dish were counted, and the number of cells per dish was used to calculate the volume of 1M ascorbic acid solution to treat the cells at 20 pmol/cell. For

in vivo studies, the volume of ascorbic acid to be injected intraperitoneally was calculated based on a 4 g kg^{-1} mouse weight dose.

4.4. Neutral and Alkaline Comet Assays

Neutral and alkaline comet assays were carried out using the R&D CometAssay Electrophoresis Starter Kit (R&D, Minneapolis, MN) following the manufacturer's instructions, with slight modifications. Briefly, cells were harvested immediately after $P\text{-AscH}^-$ treatment and resuspended in DPBS at 2×10^5 cells/mL. A total of 25 μL of cell suspension was mixed with agarose, and 50 μL of the mixture was spread on the well of a glass slide. Slides were dried in the dark at 4°C for 10 min. Slides were then incubated in cold lysis buffer for 45 min at 4°C . Following lysis, slides were incubated in a neutral buffer for 15 min or alkaline buffer for 20 min at room temperature. Slides were subjected to electrophoresis at 21 V in the appropriate buffer for 40 min for the neutral assay and 30 min for the alkaline assay. Slides were washed in water twice for 5 min, then in 70% ethanol for 5 min. Then, the slides were completely dried at 37°C for 15 min. Slides were stained with 1X SYBR Gold (ThermoFisher, Waltham, MA, USA) for 30 min at room temperature in the dark. Excess stain was removed, and slides were briefly rinsed in water before allowing them to dry at 37°C for 10 min. Fluorescent microscopy was used to image comets, and data were analyzed using the autoanalyzer software CometScore 2.0.0.38 to obtain percent tail DNA (<http://rexhoover.com/index.php?id=cometscore>, accessed: 21 December 2021).

4.5. Hydrogen Peroxide Removal Assay

The rate (k_{cell}) of the removal of extracellular H_2O_2 by different subtypes of GBM was determined using the para-hydroxyphenylacetic acid (pHPA) plate reader assay as described previously [41,42]. A total of 50,000 cells from various subtypes of GBM were seeded per well of a 96-well (Costar Clear) bottom plate. Cells were incubated for at least 48 h at 37°C , 4% O_2 , and 5% CO_2 . Subsequently, 10 μM hydrogen peroxide was added to wells and the system was quenched at predetermined times to determine the concentration of H_2O_2 remaining in the wells using a quenching solution of horseradish peroxidase (HRP) that reacts with H_2O_2 . This reaction of HRP with H_2O_2 activates HRP and subsequently oxidizes pHPA, resulting in a fluorescent dimer that corresponds to the H_2O_2 remaining in each well. Cells in each well were counted using a hemocytometer and the observed k_{cell} was determined.

4.6. Catalase Activity Assay

Catalase activity was determined using Abei's method via UV-Vis spectroscopy, detecting the disappearance of H_2O_2 at 240 nm, $\epsilon_{240} = 39.4 \text{ M}^{-1} \text{ cm}^{-1}$ [43]. A total of 55.6 mM potassium phosphate buffer (pH 7.0) was used as the working buffer for this assay. The catalase reaction was initiated by adding an excess of 30 mM H_2O_2 to a final concentration of 10 mM in the assay cuvette. The absorbance of hydrogen peroxide was monitored immediately upon the start of the reaction for 120 s (s) at 10 s intervals. The natural log of the rate of H_2O_2 disappearance was then used to determine the kU of activity. Activity was then normalized to protein content in the sample as measured using the DC Protein Assay Kit (Bio-Rad, Hercules, CA, USA).

4.7. Glutathione Peroxidase Activity Assay

Glutathione peroxidase 1 (GPx) activity was determined spectrophotometrically using the method of Lawrence and Burk [44]. Briefly, in a buffer containing reduced glutathione (1 mM), glutathione reductase (1 E.U./mL), and NADPH (0.2 mM), activity in samples or standards was determined by measuring the disappearance of NADPH at 340 nm following the addition of H_2O_2 (final concentration = 0.25 mM). A unit of GPx activity was defined as 1 μmole of NADPH oxidized/min. Activity was then normalized to protein content in the sample as measured using the DC Protein Assay Kit.

4.8. U87 Xenograft Murine Model

Female 6–8-week-old athymic nude mice (Envigo, Indianapolis, IN, USA) were used for this study. All procedures were approved by the University of Iowa Institutional Animal Care and Use Committee and conformed to NIH guidelines (IACUC protocol #0121207). Animals were kept at the University of Iowa animal care facility in a temperature-controlled environment with a 12 h light/12 h dark cycle. In total, 2×10^6 U87 GBM cells were subcutaneously injected into the right flanks of nude mice. Upon the formation of palpable tumors, animals were randomly assigned to the following groups: control, SOC, Sequence 1, and Sequence 2 (Table 2). Ionizing radiation (IR) was delivered in 2 Gy fractions to the flank for a total of 12 Gy using the University of Iowa Xstrahl small animal radiation research platform. Temozolomide (TMZ) was delivered intraperitoneally at 2.5 mg kg^{-1} . P-AscH⁻ was administered intraperitoneally at 4 g kg^{-1} . Treatment consisted of two active treatment weeks followed by two adjuvant weeks. Dosing frequencies are shown in Table 1. A tumor volume $> 1500 \text{ mm}^3$ or tumors with necrotic ulceration were considered criteria for euthanasia.

4.9. Statistical Analysis

A one-way ANOVA with the Brown–Forsythe test was used to analyze colony formation assays, hydrogen peroxide removal assay, catalase activity, and GPx activity. Paired two-tailed t-tests were performed to analyze DNA damage data. Tumor growth rate and body weight data were analyzed using a two-way ANOVA. Overall survival data were analyzed on a Kaplan–Meier curve with the Gehan–Breslow–Wilcoxon test. GraphPad Prism 9 software was used for all statistical analyses.

Supplementary Materials: The following supporting information can be downloaded at: <https://www.mdpi.com/article/10.3390/ijms242417158/s1>.

Author Contributions: Conceptualization, A.Z., K.A.M., M.S.P. and B.G.A.; methodology, A.Z. and K.A.M.; validation, A.Z.; formal analysis, A.Z. and K.A.M.; investigation, A.Z.; resources, K.A.M., M.S.P., B.G.A., D.R.S. and J.N.S.; data curation, A.Z. and K.A.M.; writing—original draft preparation, A.Z.; writing—review and editing A.Z., K.A.M., D.R.S., J.N.S., M.S.P. and B.G.A.; visualization, A.Z. and K.A.M.; supervision, B.G.A.; project administration, K.A.M., M.S.P. and B.G.A.; funding acquisition, B.G.A. and D.R.S. All authors have read and agreed to the published version of the manuscript.

Funding: This study was funded by the National Institutes of Health (NCI-P01CA217797, NCI-R21CA270742, NCI-P30CA086862, NCI-T32CA078586), Gateway for Cancer Research G-17-1500, and the Burke family.

Institutional Review Board Statement: All procedures were approved by the University of Iowa Institutional Animal Care and Use Committee and conformed to NIH guidelines (IACUC protocol #0121207).

Data Availability Statement: Raw data are available upon request to the authors.

Acknowledgments: We would like to acknowledge Jann N. Sarkaria at the Mayo Clinic for providing patient-derived GBM cell lines used in this study. We would also like to acknowledge the Radiation Core, the Antioxidant Core, and the Small Animal Imaging Core in the Holden Comprehensive Cancer Center at the University of Iowa.

Conflicts of Interest: The authors declare no conflict of interest.

References

1. Ostrom, Q.T.; Cioffi, G.; Gittleman, H.; Patil, N.; Waite, K.; Kruchko, C.; Barnholtz-Sloan, J.S. CBTRUS Statistical Report: Primary Brain and Other Central Nervous System Tumors Diagnosed in the United States in 2012–2016. *Neuro-Oncol.* **2019**, *21* (Suppl. S5), v1–v100. [CrossRef]
2. Wen, P.Y.; Kesari, S. Malignant Gliomas in Adults. *N. Engl. J. Med.* **2008**, *359*, 492–507. [CrossRef]

3. Stupp, R.; Mason, W.P.; van den Bent, M.J.; Weller, M.; Fisher, B.; Taphoorn, M.J.B.; Belanger, K.; Brandes, A.A.; Marosi, C.; Bogdahn, U.; et al. Radiotherapy plus Concomitant and Adjuvant Temozolomide for Glioblastoma. *N. Engl. J. Med.* **2005**, *352*, 987–996. [[CrossRef](#)]
4. Ostrom, Q.T.; Cioffi, G.; Waite, K.; Kruchko, C.; Barnholtz-Sloan, J.S. CBTRUS Statistical Report: Primary Brain and Other Central Nervous System Tumors Diagnosed in the United States in 2014–2018. *Neuro-Oncology* **2021**, *23*, iii1–iii105. [[CrossRef](#)] [[PubMed](#)]
5. Li, R.; Wang, H.; Liang, Q.; Chen, L.; Ren, J. Radiotherapy for glioblastoma: Clinical issues and nanotechnology strategies. *Biomater. Sci.* **2021**, *10*, 892–908. [[CrossRef](#)] [[PubMed](#)]
6. Aiyappa-Maudsley, R.; Chalmers, A.J.; Parsons, J.L. Factors affecting the radiation response in glioblastoma. *Neuro-Oncology Adv.* **2022**, *4*, vda156. [[CrossRef](#)] [[PubMed](#)]
7. Gutierrez-Quintana, R.; Walker, D.J.; Williams, K.J.; Forster, D.M.; Chalmers, A.J. Radiation-induced neuroinflammation: A potential protective role for poly(ADP-ribose) polymerase inhibitors? *Neurooncol. Adv.* **2022**, *4*, vda190. [[CrossRef](#)] [[PubMed](#)]
8. Turnquist, C.; Harris, B.T.; Harris, C.C. Radiation-induced brain injury: Current concepts and therapeutic strategies targeting neuroinflammation. *Neuro-Oncology Adv.* **2020**, *2*, vdaa057. [[CrossRef](#)] [[PubMed](#)]
9. Ahmed, M.; Canney, M.; Carpentier, A.; Idbaih, A. Overcoming the blood brain barrier in glioblastoma: Status and future perspective. *Rev. Neurol.* **2023**, *179*, 430–436. [[CrossRef](#)]
10. Ou, A.; Yung, W.K.A.; Majd, N. Molecular Mechanisms of Treatment Resistance in Glioblastoma. *Int. J. Mol. Sci.* **2020**, *22*, 351. [[CrossRef](#)]
11. Lam, M.S.; Aw, J.J.; Tan, D.; Vijayakumar, R.; Lim, H.Y.G.; Yada, S.; Pang, Q.Y.; Barker, N.; Tang, C.; Ang, B.T.; et al. Unveiling the Influence of Tumor Microenvironment and Spatial Heterogeneity on Temozolomide Resistance in Glioblastoma Using an Advanced Human In Vitro Model of the Blood-Brain Barrier and Glioblastoma. *Small* **2023**, e2302280. [[CrossRef](#)] [[PubMed](#)]
12. Chen, Q.; Espey, M.G.; Sun, A.Y.; Pooput, C.; Kirk, K.L.; Krishna, M.C.; Khosh, D.B.; Drisko, J.; Levine, M. Pharmacologic doses of ascorbate act as a prooxidant and decrease growth of aggressive tumor xenografts in mice. *Proc. Natl. Acad. Sci. USA* **2008**, *105*, 11105–11109. [[CrossRef](#)] [[PubMed](#)]
13. Schoenfeld, J.D.; Alexander, M.S.; Waldron, T.J.; Sibenaller, Z.A.; Spitz, D.R.; Buettner, G.R.; Allen, B.G.; Cullen, J.J. Pharmacological Ascorbate as a Means of Sensitizing Cancer Cells to Radio-Chemotherapy While Protecting Normal Tissue. *Semin. Radiat. Oncol.* **2018**, *29*, 25–32. [[CrossRef](#)]
14. Alexander, M.S.; Wilkes, J.G.; Schroeder, S.R.; Buettner, G.R.; Wagner, B.A.; Du, J.; Gibson-Corley, K.; O’leary, B.R.; Spitz, D.R.; Buatti, J.M.; et al. Pharmacologic Ascorbate Reduces Radiation-Induced Normal Tissue Toxicity and Enhances Tumor Radiosensitization in Pancreatic Cancer. *Cancer Res.* **2018**, *78*, 6838–6851. [[CrossRef](#)] [[PubMed](#)]
15. Zaher, A.; Stephens, L.M.; Miller, A.M.; Hartwig, S.M.; Stolwijk, J.M.; Petronek, M.S.; Zacharias, Z.R.; Wadas, T.J.; Monga, V.; Cullen, J.J.; et al. Pharmacological ascorbate as a novel therapeutic strategy to enhance cancer immunotherapy. *Front. Immunol.* **2022**, *13*, 989000. [[CrossRef](#)]
16. Schoenfeld, J.D.; Sibenaller, Z.A.; Mapuskar, K.A.; Wagner, B.A.; Cramer-Morales, K.L.; Furqan, M.; Sandhu, S.; Carlisle, T.L.; Smith, M.C.; Abu Hejleh, T.; et al. O₂– and H₂O₂-Mediated Disruption of Fe Metabolism Causes the Differential Susceptibility of NSCLC and GBM Cancer Cells to Pharmacological Ascorbate. *Cancer Cell* **2017**, *31*, 487–500.e8. [[CrossRef](#)] [[PubMed](#)]
17. Chen, Q.; Espey, M.G.; Krishna, M.C.; Mitchell, J.B.; Corpe, C.P.; Buettner, G.R.; Shacter, E.; Levine, M. Pharmacologic ascorbic acid concentrations selectively kill cancer cells: Action as a pro-drug to deliver hydrogen peroxide to tissues. *Proc. Natl. Acad. Sci. USA* **2005**, *102*, 13604–13609. [[CrossRef](#)]
18. Petronek, M.; Stolwijk, J.; Murray, S.; Steinbach, E.; Zakharia, Y.; Buettner, G.; Spitz, D.; Allen, B. Utilization of redox modulating small molecules that selectively act as pro-oxidants in cancer cells to open a therapeutic window for improving cancer therapy. *Redox Biol.* **2021**, *42*, 101864. [[CrossRef](#)]
19. Petronek, M.S.; Monga, V.; Bodeker, K.L.; Kwofie, M.; Lee, C.-Y.; Mapuskar, K.A.; Stolwijk, J.M.; Zaher, A.; Wagner, B.A.; Smith, M.C.; et al. Magnetic resonance imaging of iron metabolism with T2* mapping predicts an enhanced clinical response to pharmacological ascorbate in patients with GBM. *Clin. Cancer Res.* **2023**, ahead of print. [[CrossRef](#)] [[PubMed](#)]
20. Verhaak, R.G.W.; Hoadley, K.A.; Purdom, E.; Wang, V.; Wilkerson, M.D.; Miller, C.R.; Ding, L.; Golub, T.; Jill, P.; Alexe, G.; et al. Integrated Genomic Analysis Identifies Clinically Relevant Subtypes of Glioblastoma Characterized by Abnormalities in PDGFRA, IDH1, EGFR, and NF1. *Cancer Cell* **2010**, *17*, 98–110. [[CrossRef](#)]
21. Wang, Q.; Hu, B.; Hu, X.; Kim, H.; Squatrito, M.; Scarpace, L.; deCarvalho, A.C.; Lyu, S.; Li, P.; Li, Y.; et al. Tumor Evolution of Glioma-Intrinsic Gene Expression Subtypes Associates with Immunological Changes in the Microenvironment. *Cancer Cell* **2017**, *32*, 42–56.e46. [[CrossRef](#)] [[PubMed](#)]
22. Phillips, H.S.; Kharbanda, S.; Chen, R.; Forrest, W.F.; Soriano, R.H.; Wu, T.D.; Misra, A.; Nigro, J.M.; Colman, H.; Soroceanu, L.; et al. Molecular subclasses of high-grade glioma predict prognosis, delineate a pattern of disease progression, and resemble stages in neurogenesis. *Cancer Cell* **2006**, *9*, 157–173. [[CrossRef](#)] [[PubMed](#)]
23. Henle, E.S.; Linn, S. Formation, Prevention, and Repair of DNA Damage by Iron/Hydrogen Peroxide. *J. Biol. Chem.* **1997**, *272*, 19095–19098. [[CrossRef](#)] [[PubMed](#)]
24. Duarte, T.L.; Almeida, G.M.; Jones, G.D. Investigation of the role of extracellular H₂O₂ and transition metal ions in the genotoxic action of ascorbic acid in cell culture models. *Toxicol. Lett.* **2007**, *170*, 57–65. [[CrossRef](#)]
25. Du, J.; Cieslak, J.A., 3rd; Welsh, J.L.; Sibenaller, Z.A.; Allen, B.G.; Wagner, B.A.; Kalen, A.L.; Doskey, C.M.; Strother, R.K.; Button, A.M.; et al. Pharmacological Ascorbate Radiosensitizes Pancreatic Cancer. *Cancer Res.* **2015**, *75*, 3314–3326. [[CrossRef](#)] [[PubMed](#)]

26. Herst, P.M.; Broadley, K.W.R.; Harper, J.L.; McConnell, M.J. Pharmacological concentrations of ascorbate radiosensitize glioblastoma multiforme primary cells by increasing oxidative DNA damage and inhibiting G2/M arrest. *Free Radic. Biol. Med.* **2012**, *52*, 1486–1493. [[CrossRef](#)]
27. Zhou, L.; Zhang, L.; Wang, S.; Zhao, B.; Lv, H.; Shang, P. Labile iron affects pharmacological ascorbate-induced toxicity in osteosarcoma cell lines. *Free Radic. Res.* **2020**, *54*, 385–396. [[CrossRef](#)]
28. Rivière, J.; Ravanat, J.-L.; Wagner, J.R. Ascorbate and H₂O₂ induced oxidative DNA damage in Jurkat cells. *Free Radic. Biol. Med.* **2006**, *40*, 2071–2079. [[CrossRef](#)]
29. Ma, E.; Chen, P.; Wilkins, H.M.; Wang, T.; Swerdlow, R.H.; Chen, Q. Pharmacologic ascorbate induces neuroblastoma cell death by hydrogen peroxide mediated DNA damage and reduction in cancer cell glycolysis. *Free Radic. Biol. Med.* **2017**, *113*, 36–47. [[CrossRef](#)]
30. Behnan, J.; Finocchiaro, G.; Hanna, G. The landscape of the mesenchymal signature in brain tumours. *Brain* **2019**, *142*, 847–866. [[CrossRef](#)]
31. Fedele, M.; Cerchia, L.; Pegoraro, S.; Sgarra, R.; Manfioletti, G. Proneural-Mesenchymal Transition: Phenotypic Plasticity to Acquire Multitherapy Resistance in Glioblastoma. *Int. J. Mol. Sci.* **2019**, *20*, 2746. [[CrossRef](#)]
32. Cannan, W.J.; Pederson, D.S. Mechanisms and Consequences of Double-Strand DNA Break Formation in Chromatin. *J. Cell. Physiol.* **2015**, *231*, 3–14. [[CrossRef](#)]
33. Freifelder, D.; Trumbo, B. Matching of single-strand breaks to form double-strand breaks in DNA. *Biopolymers* **1972**, *11*, 1116. [[CrossRef](#)]
34. Nordberg, J.; Arnér, E.S. Reactive oxygen species, antioxidants, and the mammalian thioredoxin system. *Free Radic. Biol. Med.* **2001**, *31*, 1287–1312. [[CrossRef](#)]
35. Petronek, M.; Teferi, N.; Caster, J.; Stolwijk, J.; Zaher, A.; Buatti, J.; Hasan, D.; Wafa, E.; Salem, A.; Gillan, E.; et al. Magnetite nanoparticles as a kinetically favorable source of iron to enhance GBM response to chemoradiosensitization with pharmacological ascorbate. *Redox Biol.* **2023**, *62*, 102651. [[CrossRef](#)]
36. Reiber, H.; Ruff, M.; Uhr, M. Ascorbate concentration in human cerebrospinal fluid (CSF) and serum. Intrathecal accumulation and CSF flow rate. *Clin. Chim. Acta* **1993**, *217*, 163–173. [[CrossRef](#)]
37. Turner, N.; Farrow, B.; Betrie, A.H.; Finnis, M.E.; Lankadeva, Y.R.; Sharman, J.; Tan, P.; Abdelhamid, Y.A.; Deane, A.M.; Plummer, M.P. Cerebrospinal fluid and plasma ascorbate concentrations following subarachnoid haemorrhage. *Crit. Care Resusc.* **2023**. [[CrossRef](#)]
38. Heinz-Erian, P.; Achmüller, M.; Berger, H.; Bonjour, J.P.; Gasser, R.; Hornig, D.; Nirk, S.; Schneeberger, H. Cerebrospinal fluid and plasma levels of vitamin C in children. *Pediatr. Padol.* **1985**, *20*, 49–54.
39. Kaffes, I.; Szulzewsky, F.; Chen, Z.; Herting, C.J.; Gabanic, B.; Vega, J.E.V.; Shelton, J.; Switchenko, J.M.; Ross, J.L.; McSwain, L.F.; et al. Human Mesenchymal glioblastomas are characterized by an increased immune cell presence compared to Proneural and Classical tumors. *Oncol Immunology* **2019**, *8*, e1655360. [[CrossRef](#)]
40. Franken, N.A.P.; Rodermond, H.M.; Stap, J.; Haveman, J.; Van Bree, C. Clonogenic assay of cells in vitro. *Nat. Protoc.* **2006**, *1*, 2315–2319. [[CrossRef](#)]
41. Wagner, B.A.; Witmer, J.R.; Erve, T.J.V.; Buettner, G.R. An assay for the rate of removal of extracellular hydrogen peroxide by cells. *Redox Biol.* **2013**, *1*, 210–217. [[CrossRef](#)] [[PubMed](#)]
42. Doskey, C.M.; Buranasudja, V.; Wagner, B.A.; Wilkes, J.G.; Du, J.; Cullen, J.J.; Buettner, G.R. Tumor cells have decreased ability to metabolize H₂O₂: Implications for pharmacological ascorbate in cancer therapy. *Redox Biol.* **2016**, *10*, 274–284. [[CrossRef](#)] [[PubMed](#)]
43. Aebi, H. Catalase in vitro. *Methods Enzym.* **1984**, *105*, 121–126. [[CrossRef](#)]
44. Lawrence, R.A.; Burk, R.F. Glutathione peroxidase activity in selenium-deficient rat liver. *Biochem. Biophys. Res. Commun.* **1976**, *71*, 952–958. [[CrossRef](#)]

Disclaimer/Publisher’s Note: The statements, opinions and data contained in all publications are solely those of the individual author(s) and contributor(s) and not of MDPI and/or the editor(s). MDPI and/or the editor(s) disclaim responsibility for any injury to people or property resulting from any ideas, methods, instructions or products referred to in the content.